Dynamic structure of lipid-bound synaptobrevin suggests a nucleation-propagation mechanism for trans-SNARE complex formation

Jeffrey F. Ellena[a], Binyong Liang[b], Maciej Wiktor[b,c], Alexander Stein[d], David S. Cafiso[e], Reinhard Jahn[d], and Lukas K. Tamm[b,1]

[a]Biomolecular Magnetic Resonance Research Core, P.O. Box 800741, University of Virginia, Charlottesville, VA 22908; [b]Center for Membrane Biology and Department of Molecular Physiology and Biological Physics, University of Virginia, P.O. Box 800886, Charlottesville, VA 22908; [c]Department of Structural Biology, Biozentrum, University of Basel, Klingelbergstrasse 50/70, 4056 Basel, Switzerland; [d]Department of Neurobiology, Max Planck Institute for Biophysical Chemistry, Am Fassberg 11, 37077 Göttingen, Germany; and [e]Department of Chemistry, McCormick Road, University of Virginia, Charlottesville, VA 22904

Edited by Axel T Brunger, Stanford University, Stanford, CA, and approved October 6, 2009 (received for review July 27, 2009)

The synaptic vesicle protein synaptobrevin engages with syntaxin and SNAP-25 to form the SNARE complex, which drives membrane fusion in neuronal exocytosis. In the SNARE complex, the SNARE motif of synaptobrevin forms a 55-residue helix, but it has been assumed to be mostly unstructured in its prefusion form. NMR data for full-length synaptobrevin in dodecylphosphocholine micelles reveals two transient helical segments flanked by natively disordered regions and a third more stable helix. Transient helix I comprises the most N-terminal part of the SNARE motif, transient helix II extends the SNARE motif into the juxtamembrane region, and the more stable helix III is the transmembrane domain. These helices may have important consequences for SNARE complex folding and fusion: helix I likely forms a nucleation site, the C-terminal disordered SNARE motif may act as a folding arrest signal, and helix II likely couples SNARE complex folding and fusion.

structure | dynamics | membrane fusion | SNARE proteins | NMR

Synaptic release of neurotransmitter requires the docking and fusion of synaptic vesicles at the presynaptic membrane. The fusion reaction is thought to be mediated by the formation of the SNARE complex from its components syntaxin-1a and SNAP-25 in the target membrane and synaptobrevin-2 (Syb) in the vesicle membrane (1). These three proteins together form a complex that consists of a thermally very stable coiled-coil four-helix bundle, as revealed by the crystal structure of the soluble SNARE core complex (2). SNAP-25 contributes two helices to this complex and syntaxin and synaptobrevin each contribute one. More recently, the structure of the postfusion *cis*-SNARE complex with its C-terminal transmembrane (TM) domain extensions was solved at 3.4 Å resolution (3). Most interestingly, the helices continue through the juxtamembrane linker region and into the membrane, suggesting that force could be transmitted through this region into the membrane leading to membrane bending and eventually membrane fusion. This interesting finding immediately raises the question: how exactly is the assembly and folding of the four-helix bundle coupled into the membrane and how does the energy derived from this reaction ultimately fuse two different membranes into one? A common notion is that an initial *trans*-SNARE complex forms by pairing vesicle and target membrane SNAREs from their N-terminal ends and progressively folds in a zipper-like fashion toward the C-terminal TM domains. This reaction is thought to pull the two membranes into closer contact until, at some stage they merge into a single membrane. However, structural data on a *trans*-SNARE complex do not yet exist. It is also not yet known whether zipper-folding of *trans*-SNARE complexes progresses smoothly and continuously into the membrane or whether this reaction is discontinuous and segmented in some fashion.

To understand how the SNARE complex is formed and to find possible reaction intermediates, several structural studies of SNARE proteins in isolation or in binary complexes have been performed. The soluble domains of neuronal Syb (residues 1–96) (4, 5) and its yeast homolog Snc1 (6) have been found by CD and NMR spectroscopy to be mostly unstructured in aqueous solution. The TM domain of Syb was polymorphic and showed different degrees of α-helical and β-sheet secondary structures depending on environmental conditions when modeled as a short peptide comprising Syb residues 97–112 and analyzed by FTIR and CD spectroscopy (7). A more recent FTIR and CD study of the full-length Syb(1–116) concluded that the TM domain is an α-helix that is inclined 30–40° from the membrane normal and that the entire cytoplasmic domain is natively disordered (8). The cytoplasmic domain of Syb(1–116) was also found to be disordered when analyzed by site-directed spin label EPR spectroscopy (9). NMR, CD, and EPR studies showed that Syb assumes more structure when complexed with soluble syntaxin fragments (4, 5, 9).

To elucidate structural features of full-length synaptobrevin in the presence of a membrane-mimetic environment, we have used solution NMR spectroscopy to study the structure and dynamics of Syb(1–116) in lipid micelles. The results indicate helical propensities not only in the TM domain but also in regions at the beginning and end of the SNARE motif, which likely serve, respectively, as a nucleation site for SNARE complex formation and as an element to couple SNARE complex folding with fusion.

Results

Secondary Structure of Lipid-Bound Synaptobrevin. A typical HSQC spectrum of ^{15}N,^{13}C-labeled Syb(1–116) in dodecylphosphocholine (DPC) micelles is shown in Fig. 1. Sample conditions were optimized as described in *SI Experimental Procedures* and yielded the highest quality spectra at a protein:lipid ratio of 1:200 and a recording temperature of 45 °C. Variable peak intensities in this spectrum indicate that different residues may experience different rotational correlation times, possibly because of different degrees of association with the lipid micelles. Of the 108 non-proline residues, 106 were assigned from the Cα, Cβ, and CO backbone connectivities obtained from HNCA, HNCACB, HNCO, HN(CA)CO, and CBCA(CO)NH experiments and a ^{15}N-edited NOESY experiment. Met-1 and Asp-40 were the only residues that

Author contributions: J.F.E., B.L., D.S.C., R.J., and L.K.T. designed research; J.F.E., B.L., M.W., and A.S. performed research; J.F.E., B.L., D.S.C., and L.K.T. analyzed data; and J.F.E., B.L., and L.K.T. wrote the paper.

The authors declare no conflict of interest.

This article is a PNAS Direct Submission.

Data deposition: The atomic coordinates have been deposited in the Protein Data Bank, www.pdb.org (PDB ID code 2KOG).

[1]To whom correspondence should be addressed. E-mail: lkt2e@virginia.edu.

This article contains supporting information online at www.pnas.org/cgi/content/full/0908317106/DCSupplemental.

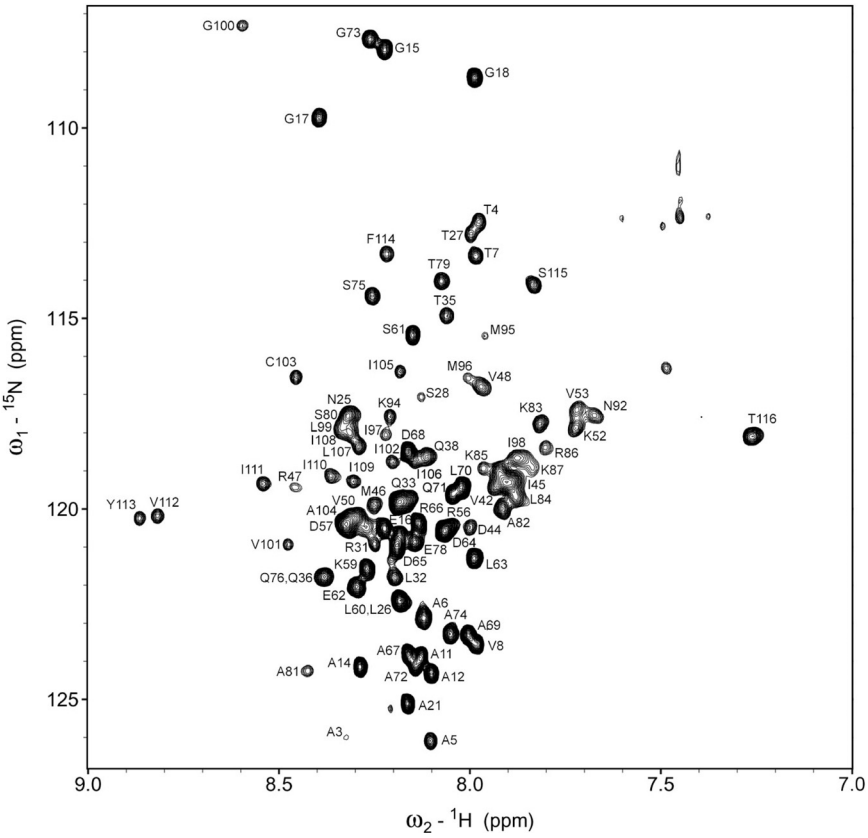

Fig. 1. ^{15}N-^{1}H HSQC spectrum of Syb(1–116) in DPC micelles at pH 6.0 and 45 °C, measured at 600 MHz. Assignments of backbone amides are denoted by one letter amino acid abbreviations followed by their sequence numbers.

remained only partially assigned (Cα and Cβ assignments complete). We also studied the shorter membrane-bound fragment Syb(60–116), which was independently completely assigned from triple-resonance experiments (Fig. S1). The chemical shifts of Syb(60–116) were very similar to those of the corresponding residues in Syb(1–116), except for residues 60–63, which are internal in full-length Syb, but form the N terminus of the fragment.

The Cα and Cβ chemical shifts were used to estimate elements of secondary structure of Syb(1–116). Fig. 2*A* shows three-residue averaged (ΔCα–ΔCβ) secondary chemical shifts plotted as a function of amino acid sequence number. The pattern in Fig. 2*A* clearly indicates that there are three regions that likely form α-helices: residues 36–54 (helix I), 77–88 (helix II), and 93–115 (helix III). Helix I covers a good portion of the N-terminal half of the SNARE motif, which encompasses residues 28–84. Helix II covers the C-terminal end of the SNARE motif, but extends about one turn longer into the juxtamembrane domain. Helix III corresponds to the TM domain.

Comparison with the Soluble Fragment Syb(1–96). An earlier NMR study of human Syb(1–96) indicated that this soluble fragment is unstructured, except for perhaps a hint of some helical structure near the C terminus (5). We prepared the same fragment of rat synaptobrevin and essentially reproduced the earlier data (Fig. 2*C*). The HSQC spectrum of Syb(1–96) in buffer revealed almost uniform peak intensities and linewidths (Fig. S2). All resonances were assigned from triple-resonance experiments. Except for a few residues around the single amino acid substitution from the human to the rat sequence (Ala-8 becomes a Val), the chemical shifts of the human and rat datasets are in excellent agreement.

When the same fragment was measured in the presence of DPC micelles, the NMR spectra changed dramatically. Many resonances disappeared in the HSQC spectrum at 18 °C, but gradually reappeared at higher temperatures. This process was fully reversible. A representative fully assigned (from triple-resonance backbone experiments) HSQC spectrum collected at 45 °C is shown in Fig. S3. As with Syb(1–116), peak intensities and linewidths varied, indicative of different rotational correlation times for different residues. The secondary chemical shift plot (Fig. 2*B*) indicates a significant induction of secondary structure by the presence of DPC micelles. The remarkable resemblance of secondary chemical shifts between Syb(1–116) and Syb(1–96) in DPC shows that the structure of the soluble domain of Syb is very similar in DPC micelles, irrespective of whether it is anchored in micelles with a TM domain or not.

Backbone Dynamics of Free and Lipid-Bound Synaptobrevin. To probe the backbone dynamics, heteronuclear {^{1}H}-^{15}N NOEs of Syb(1–116) in DPC micelles were recorded. Since the theoretical rigid limit for {^{1}H}-^{15}N NOEs at 800 MHz is 0.86 (10), values greater than approximately 0.5 indicate restricted backbone motions, and smaller positive and negative values indicate extended backbone motions on the ps-ns time-scale. All three proposed α-helices showed relatively high {^{1}H}-^{15}N NOE values (Fig. 3*B*). The average values were 0.54, 0.51, and 0.78 for residues comprising helices I, II, and III, respectively. According to these data, the TM region is the most rigid of these segments. Helices I and II are more flexible, although they are clearly not as dynamic as the rest of protein. Based on the negative heteronuclear NOEs, the proline-rich N terminus is particularly dynamic.

These conclusions are further supported by NMR relaxation experiments. Backbone ^{15}N spin-lattice (Fig. 3*C*) and spin-spin (Fig. 3*D*) relaxation rates were measured. Helices I and III exhibited decreased R_1 rates averaging 1.24 s^{-1} and 0.77 s^{-1}, respectively, compared to helix II and nonhelical residues (1.77 s^{-1} and 1.67 s^{-1}, respectively). By contrast, helices I, II, and III had R_2 rates of 14.2, 12.1, and 23.5 s^{-1}, respectively, compared to 5.71 s^{-1} for disordered regions. The relatively high R_2 and low

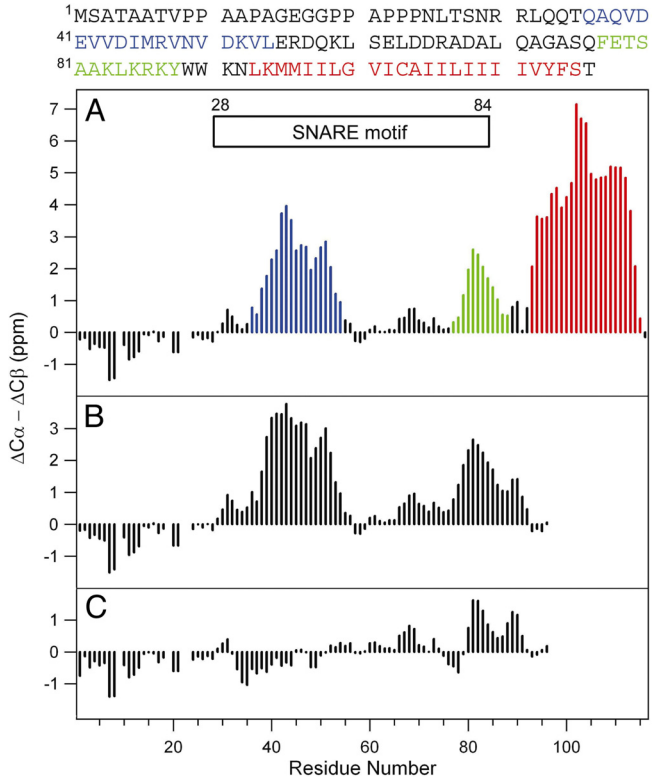

Fig. 2. Three-bond averaged secondary chemical shifts, where $(\Delta C^{\alpha} - \Delta C^{\beta})_i = 1/3(\Delta C^{\alpha}_{i-1} + \Delta C^{\alpha}_{i} + \Delta C^{\alpha}_{i+1} - \Delta C^{\beta}_{i-1} - \Delta C^{\beta}_{i} - \Delta C^{\beta}_{i+1})$, versus residue sequence numbers *i*. Each individual ΔC value on the right hand side of the equation is the chemical shift deviation from its respective random coil value. (*A*) Syb(1–116) in DPC micelles, (*B*) Syb(1–96) in DPC micelles, and (*C*) Syb(1–96) in aqueous solution. The SNARE motif of synaptobrevin as defined by the crystal structure of the SNARE complex (2) is shown as a box and helices I, II, and III are indicated by blue, green, and red colors in the sequence on the *Top*.

R_1 values of helices I and III indicate that these helices experience long rotational correlation times meaning that they likely rotate together with the micelle, whereas helix II has a shorter correlation time, and therefore moves more independently. The relatively high R_2 rate coupled with a lack of reduction of the R_1 rate of helix II also indicates that this helix may undergo conformational exchange on the μs-ms time-scale (11).

To further probe the conformational stability of the three helical segments of Syb(1–116), we measured amide hydrogen-exchange with water by performing a CLEANEX-PM experiment (12). Fig. 3*E* shows residues that exhibit hydrogen-exchange within 10 ms with an assigned value of +1 and residues that do not exchange after 80 ms with an assigned value of −1. Evidently, helices I and III are quite stable on this time-scale, whereas helix II and the juxtamembrane domain are solvent accessible, as is the rest of the protein.

Hydropathy and Helical Wheel Analysis. A hydropathy and hydrophobic moment analysis (13) of the synaptobrevin sequence reveals that, as expected, the TM domain shows up as the most hydrophobic part and that a highly amphipathic helical region is centered on residue 44 (14) (Fig. S4*a*). If this region is modeled on a helical wheel, it is clear that one face of the helix is quite hydrophobic and the other face is hydrophilic and highly charged (Fig. S4*b*). Consistent with a micelle-induced formation of a stable α-helix in the N-terminal, but not in the C-terminal half of the SNARE motif, the hydrophobic moment and hydropathy profiles for the SNARE domain (residues 28–85) indicate that the C-terminal half of the domain is less amphipathic and more hydrophilic than the N-terminal half.

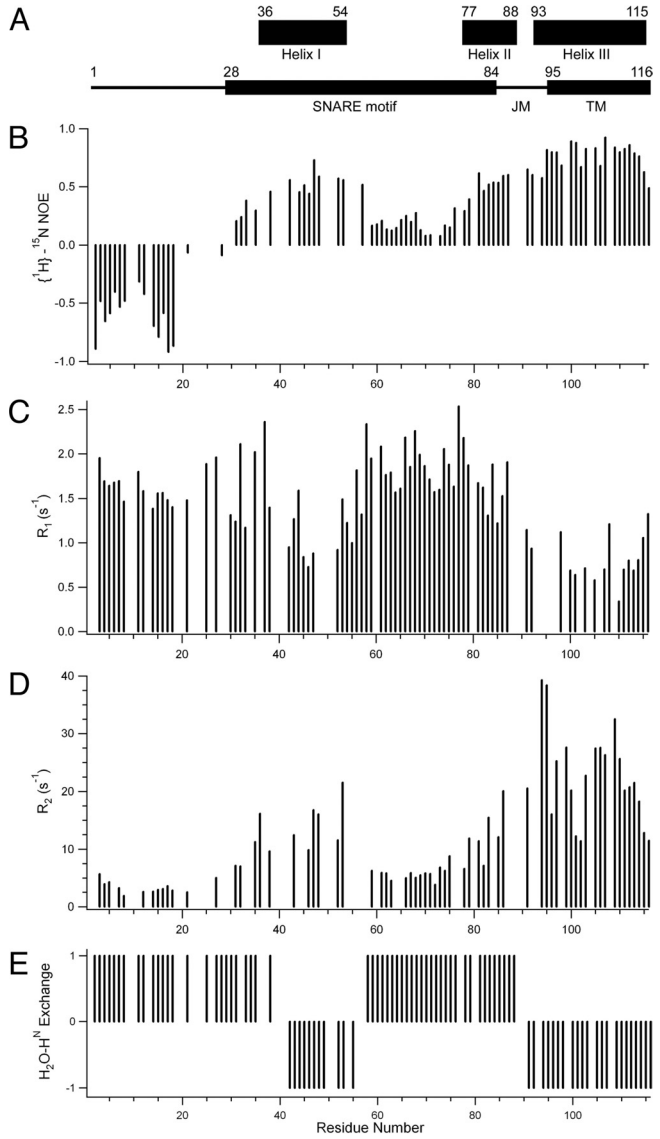

Fig. 3. Backbone dynamics of Syb(1–116) measured at 800 MHz. (*A*) *Top*: helices, as defined in this manuscript; *Bottom*: predicted domain arrangement of synaptobrevin, (*B*) Heteronuclear $\{^1H\}$-^{15}N NOEs, (*C*) ^{15}N-R_1, (*D*) ^{15}N-R_2, and (*E*) water-amide proton exchange. In (*E*), the residues undergoing fast (<10 ms) exchange are given a value of +1, and the residues undergoing slow (>80 ms) or no exchange are given a value of −1.

Structure of Synaptobrevin in DPC Micelle. One hundred structures of Syb(1–116) in DPC micelles were calculated from TALOS-derived dihedral angle, NOE-derived distance, and hydrogen-bond restraints as described in *SI Experimental Procedures*. The 20 lowest energy structures were analyzed and the structural statistics are summarized in Table S1. As expected from the described chemical shift and dynamical data, the structure of synaptobrevin is characterized by three helices connected by two flexible natively disordered domains and a highly flexible proline-rich N-terminal tail (Fig. 4). The TM helix (helix III) comprising residues 93–115 is a couple of residues longer at the N terminus than what might be expected from simple hydropathy analysis. It is slightly bent with about six helical turns that align very well in all structures (Fig. 4*D*) (backbone rmsd of 0.62 ± 0.18 Å). Not surprisingly, the interfacial residues Leu-93, Lys-94, Ser-115, and Thr-116 are a little less well ordered compared to the rest of the helix.

The next most prominent helix is the amphipathic helix I that

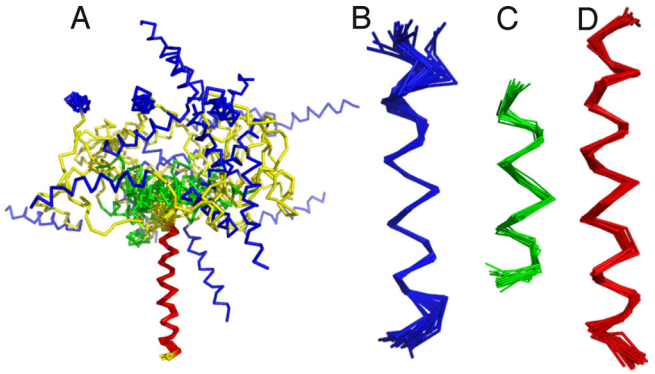

Fig. 4. Twenty lowest energy structures of Syb(1–116) in DPC micelles. Residues 36–54 are blue, 77–88 are green, 93–115 are red, and the rest are yellow. (*A*) Residues 36–116 aligned along TM domain (residues 93–115). (*B*) Helix I (residues 36–54) aligned (rmsd 1.03 ± 0.29 Å) (*C*) Helix II (residues 77–88) aligned (rmsd 0.81 ± 0.29 Å). (*D*) Transmembrane helix III (residues 93–115) aligned (rmsd 0.62 ± 0.18 Å). N-terminals are at the *Top* in *B*, *C*, and *D*.

spans residues 36–54, with a backbone rmsd of 1.03 ± 0.29 Å (Fig. 4*B*). Helix II, which comprises the end of the SNARE motif and leads into the juxtamembrane domain, i.e., residues 77–88, is well defined (Fig. 4*C*) (rmsd 0.81 ± 0.29 Å), although it undergoes quite fast amide hydrogen-exchange on the 10-ms time scale (Fig. 3*E*).

It is interesting to note that helices II and III are connected by only four residues, namely Trp-89, Trp-90, Lys-91, and Asn-92, which apparently form a flexible hinge at the micelle surface, and by inference, at the membrane-water interface. This hinge allows helix II to emanate from the micelle or membrane surface in many different directions as is evident from Fig. 4*A*.

Most of the C-terminal half of the SNARE motif (i.e., residues 55–76) is natively disordered. Even though the N-terminal half of the SNARE motif (helix I) interacts with the micelle and presumably the membrane surface and, therefore, has to bend back toward an interface, this helix samples many different orientations relative to the TM domain owing to the flexible nature of the C-terminal portion of the SNARE motif.

Fig. 5 shows a ribbon diagram of the lowest energy structure of Syb(1–116) in DPC micelles. One can position this structure so that the amphipathic helix I lies at a membrane interface, helix III is on

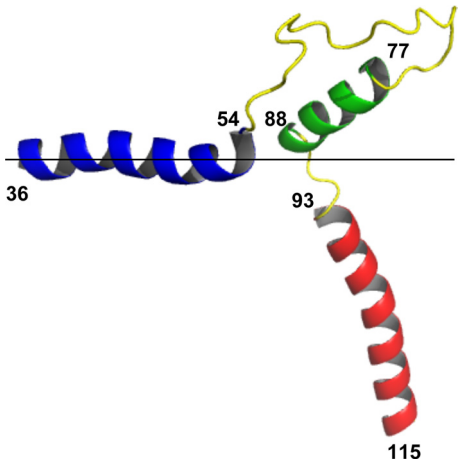

Fig. 5. Ribbon representation of lowest energy structure of Syb(1–116) in DPC micelles. This structure conforms well to the plane of a membrane, the interface of which is shown as a line. Helices I, II, and III are colored in blue, green, and red as in the sequence and secondary chemical shift plots of Fig. 2. For simplicity, the natively disordered N-terminal tail (residues 1–35) is not shown. A version of Fig. 5 with residues 1–35 included is shown in Fig. S6.

the hydrophobic side of the interface and rest of the molecule is almost completely on the hydrophilic side of the interface, as shown in Fig. 5. Not all structures in the structural ensemble can be positioned in this way. Due to the flexible nature of the molecule and the lack of long-range structural restraints many structures have their amphipathic helices projected into different directions relative to a hypothetical membrane plane. Since our data were collected in DPC micelles at a protein:lipid ratio of 1:200 and since a typical DPC micelle contains ≈40–80 lipid molecules (15), our sample contains an approximate 3- to 5-fold molar excess of micelles over protein, potentially allowing one protein to interact with more than one micelle that may not assume fixed spatial orientations relative to one another. We have attempted to measure residual dipolar couplings in several different aligning media, but were unsuccessful to prepare appropriate samples. However, even if such experiments had been successful, we suspect that the distribution of relative orientations of the helices of synatpobrevin would still be very broad due to the dynamic nature of the intervening unstructured regions.

Discussion

The structure of full-length synaptobrevin-2 in DPC micelles is segmented, dynamical, and characterized by varied structural and motional properties along the sequence. Previously, structures of postfusion *cis*-SNARE complexes comprising all three synaptic SNARE proteins or structural studies on only the soluble fragments of individual SNARE proteins have been completed (2, 3, 5, 6, 16, 17). Although based on earlier NMR studies, it was expected that the cytoplasmic domain of membrane-bound synaptobrevin would be natively disordered, we found that lipid-bound synaptobrevin contains substantial structure not only in its TM domain, but also in its SNARE motif and juxtamembrane domains even before it engages with other SNAREs to form the fusion complex. We have used the chemical shift-based secondary structure propensity method (18) to estimate fractional helical populations and find average values of 0.73 ± 0.18, 0.65 ± 0.18, and 1.2 ± 0.2 for helices I, II, and III, respectively (a value of 1 indicates a fully formed stable α-helix and a value of 0.5 means that 50% of the ensemble is α-helical). The high value for helix III is likely due to the fact that the chemical shift database used in this method is almost completely from soluble proteins and, therefore may not be appropriate for helix III. The lower values for helices I and II indicate that their conformational ensembles are predominantly helical, but that they also contain substantial unstructured fractions.

Although a previous CD and FTIR study of membrane-bound synaptobrevin emphasized the unstructured nature of its soluble domain, experiments with a shorter fragment comprising residues 74–116 is consistent with our results (8). The authors found approximately 27 residues of this fragment to be helical, which is clearly more than required for the transmembrane domain and within experimental error similar to the sum of our helices II and III, especially taking into account that helix II may not be formed all of the time. The previous EPR study on full-length synaptobrevin did not indicate helical residues in the SNARE motif (9), but the data could also be interpreted as forming a transient helix in this region. In fact, their spectra are very similar to EPR spectra of transient helical regions in the GCN4 coiled coil transcriptional activator (19) and in linker segments of rhodopsin (20). Similarly, residues 84–88 clearly show a helical period, but residues 89–92 do not, although the authors interpreted the data as a continuous interfacial helix in this region. In summary, we think that the CD data for synaptobrevin in micelles (8) and the raw EPR data for synaptobrevin in bilayers (9) are completely consistent with the current NMR data for synaptobrevin in DPC micelles and the interpretation in terms of the transient helices I and II as indicated in Figs. 4 and 5.

Interestingly, the N-terminal half of the SNARE motif of synaptobrevin is structured as an amphipathic helix when associated with membrane-mimicking micellar lipids, but the C-terminal half

of the SNARE motif remains natively disordered even in the presence of lipids. The N-terminal SNARE motif helix is induced by the presence of the lipid micelle because it is unstructured in the absence of lipids, confirming previous results (5, 6). Since synaptobrevin in synaptic vesicles is always near a membrane interface, the N-terminal SNARE motif helix observed here may also be present in its natural physiological environment. The hydrophobic face of helix I consists of the same residues which form the coiled coil heptad repeat and face the interior of the SNARE complex (2, 3). The existence of helix I (and II) is not an artifact of the high DPC concentration used in these experiments because experiments at a 40-fold lower concentration essentially produced the same result (Fig. S5). Similarly, adding 12% of the negatively charged detergent SDS to mimic negatively charged lipids in the synaptic membranes did not alter our results either (Fig. S5). A second important structural feature is a nascent α-helix at the transition from the SNARE motif to the 10-residue juxtamembrane domain (residues 85–94) that links the SNARE motif (residues 28–84) with the TM domain (residues 95–116). Even before forming a complex with cognate SNAREs, this segment adopts a helical structure in its DPC-bound prefusion form. Residues 77–88 form a helix that extends four more residues from layer +8 of the SNARE motif into the juxtamembrane domain. Similarly, the TM domain is N-terminally two residues longer than what might be expected from hydropathy analysis and includes Lys-94 whose charged side chain likely snorkels up to the micelle and membrane surface. This leaves only residues Trp-89–Asn-92 as an unstructured linker between the extended SNARE motif and TM domains.

Although a DPC micelle is not a lipid bilayer, DPC still has the same zwitterionic phosphocholine headgroup as the major membrane phospholipid phosphatidylcholine. Therefore, it is generally considered a mild detergent that largely preserves native structures of membrane proteins. Indeed, DPC is a preferred lipid for determining structures of membrane proteins by solution NMR (21–25). However, and despite the earlier NMR successes with DPC, caution is still advised when extrapolating some aspects of our synaptobrevin structure to situations in lipid bilayers. Although we believe that the general conclusions of the current work also carry over to lipid bilayers, there may be details especially in the interfacial juxtmembrane region of the protein that may not be exactly the same in the two environments. Future studies using additional methods will be needed to substantiate or refute some of these details.

The dynamics experiments shed further light on the conformational flexibility of different regions of the synaptobrevin structure. The TM helix is clearly the most rigid and stable of all three helical segments. Based on its inability to undergo amide hydrogen-exchange, the association of this helix with lipid micelles is strong. Helices I and II exhibit different dynamical behaviors. Motions on the ps-ns time-scale, as well as amide hydrogen-exchange on the 10 ms time-scale provide strong evidence that helix I, but not helix II interacts with the micelle surface. Based on the R_1 and R_2 relaxation behavior, helix II may also undergo conformational exchange on the μs-ms time-scale.

Helix I as a Nucleation Site for *trans*-SNARE Complex Formation? The existence of nascent helix I before synaptobrevin forms a complex with t-SNAREs may have significant biological consequences. It is generally accepted that SNAREs zipper from the N- toward the C-terminal ends and that this folding reaction drives membrane fusion (26–29). In accordance with this notion, the N-terminal SNARE motif helix I of synaptobrevin observed here may serve as a nucleation site for *trans*-SNARE complex formation. A preformed helix in this region would provide a mechanism to (a) speed up the process of forming the initial *trans*-SNARE complex and (b) increase the fidelity of starting SNARE complex folding at the N-terminal rather than the C-terminal end. In general, folding can be induced by binding or assembly might occur by conformational selection or some combination of the two (30). An example of conformational selection has been described in detail for the folding of the GCN4 leucine zipper coiled coil (31). If SNARE complex folding follows the model of GCN4 coiled coil folding, a preformed N-terminal helix would be kinetically advantageous.

Since the C-terminal portion of the synaptobrevin SNARE motif has a lower propensity to form an α-helix and, by inference, to pair with t-SNARE helices, zipper-folding of the *trans*-SNARE complex may transiently stop or be slowed down when it reaches this region of the protein. Thus, the C-terminal portion of the SNARE motif may serve as a "stop-folding" signal. This folding-arrested *trans*-SNARE complex may be present at the docked, but not yet fused stage of the overall reaction. An additional trigger, perhaps provided by synaptotagmin (un)binding and/or complexin dissociation, may push complex formation over the final energy barrier to proceed to completion and ultimately to membrane fusion. This model is in fact very similar to, and supports a model recently proposed for the function of complexin as a mediator of two-stage SNARE complex folding (32, 33).

Further support for this model comes from folding studies, in which the assembly and disassembly of SNARE complexes with synaptobrevin fragments of different lengths was investigated (28). In these studies, SNARE complexes with Syb25–96, Syb35–96, Syb42–96, Syb49–96, or Syb60–96 were formed and then challenged with Syb1–96. Interestingly, Syb1–96 could not replace peptides covering the N-terminal portion of helix I (Syb25–96 and Syb35–96) in the complex, but was able to exchange peptides that covered the more C-terminal portions of the SNARE motif (Syb42–96, Syb49–96, and Syb60–96). These studies and a subsequent detailed thermodynamic analysis of the interaction of various SNARE fragments (34) strongly indicate that the N-terminal portion of the sequence (helix I) contributes more to the stability of the complex than the C-terminal portions of the SNARE complex, again supporting the nucleation-propagation model of SNARE complex folding. Electrophysiological experiments using progressive SNARE layer mutants of SNAP-25 also favor a two-stage model implying separate nucleation and propagation phases of the folding reaction (29).

A structure-function study of a SNARE complex with a single site mutation near the C-terminal end of the syntaxin SNARE motif is also consistent with a lower stability and folding rate of the C-terminal compared to the N-terminal end of SNARE complex formation (35). The layer +7 T254I mutation enhances constitutive and evoked fusion and also changes the structure to one that is more similar to SNARE complexes associated with constitutive fusion.

Helix II as a Coupler of *trans*- to *cis*-SNARE Complex Conversion and Membrane Merger? Nascent helix II extends from the last SNARE motif layer +8 to the juxtamembrane domain of uncomplexed synaptobrevin. Down-stream from the above mentioned "stop-folding" signal, this helix may well transmit force from SNARE complex folding into the membrane and thus coerce the two membranes to fuse once the folding signal arrives at this stage. The subsequent 4-residue linker comprises two Trps, one Lys, and one Asn. Tryptophans are known to have a strong affinity (approximately 2 kcal/mol/residue) for membrane interfaces, which is further amplified when they occur in pairs or in tandem with other aromatic residues (36). Lysines also have a relatively long aliphatic chain before the terminal amino group and therefore can be buried quite deep in a membrane interface. Thus, this very short flexible linker region appears to be ideally designed to convert a *trans*-SNARE into a *cis*-SNARE complex, which must be coupled with merging the two membranes because the TM domains of synaptobrevin and syntaxin reside in the same membrane in the postfusion *cis*-SNARE complex. Flexibility is needed to tilt and accommodate the folding of the *trans*-SNARE complex between the two approaching membranes and shortness is needed for efficient

coupling between folding and membrane merger, possibly by injecting the linker Trp residues into the adjacent membrane. Trp-89 and Trp-90 have been claimed by some investigators to regulate SNARE assembly in membranes (9), but this notion is controversial (37).

Deletion or insertion of a small number of residues including insertion of two helix-breaking prolines in the juxtamembrane region has little or no effect on SNARE-mediated fusion, but insertion of longer flexible linkers has progressively inhibitory effects on SNARE-mediated liposome fusion in vitro (37, 38). However, quite mild and short (39), as well as more dramatic long insertions (40) have significant effects on Ca^{2+}-evoked exocytosis in cellular settings. The study by Kesavan et al. (39) clearly shows that Ca^{2+} sensitivity is not affected by the specifics of the juxtamembrane linker region, but that down-stream fusion pore initiation and expansion on the millisecond timescale critically depends on it. This suggests that membrane proximity of the SNARE motif and rapid propagation of SNARE folding through the juxtamembrane region is more critical for fast millisecond time scale fusion than it is for slow fusion that is typical in in vitro liposome fusion assays. Fast in vitro fusion assays, such as one recently developed in our laboratory (41) should shed more light on this possibility and should help reconcile the mentioned discrepancies on the mechanistic role of the linker region.

Very recently, the structure of the full-length SNARE complex including the TM domains of syntaxin and synaptobrevin was solved (3). Most interestingly, the SNARE motif helical bundle of syntaxin and synaptobrevin continues uninterrupted into the helical TM regions of these two proteins. Apparently, the transition from the pre- to the postfusion structure involves helical folding of the last four residues between the SNARE motif and TM domain of synaptobrevin. Therefore, this final folding step appears to be the major link between SNARE zippering and membrane fusion. It will be interesting to see if syntaxin in its uncomplexed form or complexed with SNAP-25 only also has a flexible linker that is as short as that of synaptobrevin. If so, this would provide an efficient mechanical device to couple SNARE complex folding with the unification of two initially separate membranes.

Materials and Methods

Expression and purification of Syb(1–116) and Syb(1–96) from *Rattus norvegicus* were performed as described in refs. 42 and 43. The final optimized NMR samples of Syb(1–116) were prepared from ^{13}C and ^{15}N-labeled proteins containing 200 mM dodecylphosphocholine (DPC), 150 mM NaCl, 5 mM DTT, 1 mM EDTA, 5% D_2O, and 20 mM Mes, pH 6.0. For the backbone and side-chain resonance assignments, a total of 10 different types of 3-D experiments were collected at 45 °C on 600 or 800 MHz spectrometers. ^{15}N-edited NOESY spectra with a mixing time of 120 ms, heteronuclear $\{^1H\}$-^{15}N NOE, ^{15}N-T_1, and T_2 measurements, and water-amide proton exchange experiments were collected at 800 MHz. All spectra were processed and analyzed with NMRPipe (44) and Sparky (45). Indirect dimensions in the 3-D experiments were processed with forward-backward linear prediction. For structural calculations, dihedral angle restraints predicted from the TALOS program (46), NOE distances from NOESY experiments, and alpha-helical backbone hydrogen bonds were used as inputs in the program Xplor-NIH (47). Details are provided in *SI Experimental Procedures* and Fig. S7.

ACKNOWLEDGMENTS. This work was supported by National Institutes of Health grant P01 GM72694.

1. Jahn R, Scheller RH (2006) SNAREs–engines for membrane fusion. *Nat Rev Mol Cell Biol* 7:631–643.
2. Sutton RB, Fasshauer D, Jahn R, Brunger AT (1998) Crystal structure of a SNARE complex involved in synaptic exocytosis at 2.4 A resolution. *Nature* 395:347–353.
3. Stein A, Weber G, Wahl MC, Jahn R (2009) Helical extension of the neuronal SNARE complex into the membrane. *Nature* 460:525–528.
4. Fasshauer D, et al. (1997) Structural changes are associated with soluble N-ethylmaleimide-sensitive fusion protein attachment protein receptor complex formation. *J Biol Chem* 272:28036–28041.
5. Hazzard J, Sudhof TC, Rizo J (1999) NMR analysis of the structure of synaptobrevin and of its interaction with syntaxin. *J Biomol NMR* 14:203–207.
6. Fiebig KM, Rice LM, Pollock E, Brunger AT (1999) Folding intermediates of SNARE complex assembly. *Nat Struct Biol* 6:117–123.
7. Langosch D, et al. (2001) Peptide mimics of SNARE transmembrane segments drive membrane fusion depending on their conformational plasticity. *J Mol Biol* 311:709–721.
8. Bowen M, Brunger AT (2006) Conformation of the synaptobrevin transmembrane domain. *Proc Natl Acad Sci USA* 103:8378–8383.
9. Kweon DH, Kim CS, Shin YK (2003) Regulation of neuronal SNARE assembly by the membrane. *Nat Struct Biol* 10:440–447.
10. Kay LE, Torchia DA, Bax A (1989) Backbone dynamics of proteins as studied by 15N inverse detected heteronuclear NMR spectroscopy: Application to staphylococcal nuclease. *Biochemistry* 28:8972–8979.
11. Jarymowycz VA, Stone MJ (2006) Fast time scale dynamics of protein backbones: NMR relaxation methods, applications, and functional consequences. *Chem Rev* 106:1624–1671.
12. Hwang TL, van Zijl PC, Mori S (1998) Accurate quantitation of water-amide proton exchange rates using the phase-modulated CLEAN chemical EXchange (CLEANEX-PM) approach with a Fast-HSQC (FHSQC) detection scheme. *J Biomol NMR* 11:221–226.
13. Eisenberg D, Weiss RM, Terwilliger TC (1982) The helical hydrophobic moment: A measure of the amphiphilicity of a helix. *Nature* 299:371–374.
14. Jahn R, Sudhof TC (1994) Synaptic vesicles and exocytosis. *Annu Rev Neurosci* 17:219–246.
15. Kallick DA, Tessmer MR, Watts CR, Li CY (1995) The use of dodecylphosphocholine micelles in solution NMR. *J Magn Reson B* 109:60–65.
16. Antonin W, et al. (2002) Crystal structure of the endosomal SNARE complex reveals common structural principles of all SNAREs. *Nat Struct Biol* 9:107–111.
17. Chen X, et al. (2002) Three-dimensional structure of the complexin/SNARE complex. *Neuron* 33:397–409.
18. Marsh JA, Singh VK, Jia Z, Forman-Kay JD (2006) Sensitivity of secondary structure propensities to sequence differences between alpha- and gamma-synuclein: Implications for fibrillation. *Protein Sci* 15:2795–2804.
19. Columbus L, Hubbell WL (2004) Mapping backbone dynamics in solution with site-directed spin labeling: GCN4–58 bZip free and bound to DNA. *Biochemistry* 43:7273–7287.
20. Altenbach C, et al. (1996) Structural features and light-dependent changes in the cytoplasmic interhelical E-F loop region of rhodopsin: A site-directed spin-labeling study. *Biochemistry* 35:12470–12478.
21. Arora A, Abildgaard F, Bushweller JH, Tamm LK (2001) Structure of outer membrane protein A transmembrane domain by NMR spectroscopy. *Nat Struct Biol* 8:334–338.
22. Oxenoid K, Chou JJ (2005) The structure of phospholamban pentamer reveals a channel-like architecture in membranes. *Proc Natl Acad Sci USA* 102:10870–10875.
23. Liang B, Tamm LK (2007) Structure of outer membrane protein G by solution NMR spectroscopy. *Proc Natl Acad Sci USA* 104:16140–16145.
24. Zhou Y, et al. (2008) NMR solution structure of the integral membrane enzyme DsbB: Functional insights into DsbB-catalyzed disulfide bond formation. *Mol Cell* 31:896–908.
25. Van Horn WD, et al. (2009) Solution nuclear magnetic resonance structure of membrane-integral diacylglycerol kinase. *Science* 324:1726–1729.
26. Melia TJ, et al. (2002) Regulation of membrane fusion by the membrane-proximal coil of the t-SNARE during zippering of SNAREpins. *J Cell Biol* 158:929–940.
27. Fasshauer D, Margittai M (2004) A transient N-terminal interaction of SNAP-25 and syntaxin nucleates SNARE assembly. *J Biol Chem* 279:7613–7621.
28. Pobbati AV, Stein A, Fasshauer D (2006) N- to C-terminal SNARE complex assembly promotes rapid membrane fusion. *Science* 313:673–676.
29. Sorensen JB, et al. (2006) Sequential N- to C-terminal SNARE complex assembly drives priming and fusion of secretory vesicles. *EMBO J* 25:955–966.
30. Wright PE, Dyson HJ (2009) Linking folding and binding. *Curr Opin Struct Biol* 19:31–38.
31. Steinmetz MO, et al. (2007) Molecular basis of coiled-coil formation. *Proc Natl Acad Sci USA* 104:7062–7067.
32. Xue M, et al. (2007) Distinct domains of complexin I differentially regulate neurotransmitter release. *Nat Struct Mol Biol* 14:949–958.
33. Giraudo CG, et al. (2009) Alternative zippering as an on-off switch for SNARE-mediated fusion. *Science* 323:512–516.
34. Wiederhold K, Fasshauer D (2009) Is assembly of the SNARE complex enough to fuel membrane fusion? *J Biol Chem* 284:13143–13152.
35. Lagow RD, et al. (2007) Modification of a hydrophobic layer by a point mutation in syntaxin 1A regulates the rate of synaptic vesicle fusion. *PLoS Biol* 5:e72.
36. Hong H, et al. (2007) Role of aromatic side chains in the folding and thermodynamic stability of integral membrane proteins. *J Am Chem Soc* 129:8320–8327.
37. Siddiqui TJ, et al. (2007) Determinants of synaptobrevin regulation in membranes. *Mol Biol Cell* 18:2037–2046.
38. McNew JA, et al. (1999) The length of the flexible SNAREpin juxtamembrane region is a critical determinant of SNARE-dependent fusion. *Mol Cell* 4:415–421.
39. Kesavan J, Borisovska M, Bruns D (2007) v-SNARE actions during Ca(2+)-triggered exocytosis. *Cell* 131:351–363.
40. Deak F, Shin OH, Kavalali ET, Sudhof TC (2006) Structural determinants of synaptobrevin 2 function in synaptic vesicle fusion. *J Neurosci* 26:6668–6676.
41. Domanska MK, et al. (2009) Single vesicle millisecond fusion kinetics reveals number of SNARE complexes optimal for fast SNARE-mediated membrane fusion. *J Biol Chem* 284:32158–32166.
42. Fasshauer D, Eliason WK, Brunger AT, Jahn R (1998) Identification of a minimal core of the synaptic SNARE complex sufficient for reversible assembly and disassembly. *Biochemistry* 37:10354–10362.
43. Schuette CG, et al. (2004) Determinants of liposome fusion mediated by synaptic SNARE proteins. *Proc Natl Acad Sci USA* 101:2858–2863.
44. Delaglio F, et al. (1995) NMRPipe: A multidimensional spectral processing system based on UNIX pipes. *J Biomol NMR* 6:277–293.
45. Goddard TD, Kneller DG (2008) SPARKY, NMR Assignment and Integration Software (Univ of California, San Francisco) Version 3.114.
46. Cornilescu G, Delaglio F, Bax A (1999) Protein backbone angle restraints from searching a database for chemical shift and sequence homology. *J Biomol NMR* 13:289–302.
47. Schwieters CD, Kuszewski JJ, Tjandra N, Clore GM (2003) The Xplor-NIH NMR molecular structure determination package. *J Magn Reson* 160:65–73.

Supporting Information

Ellena et al. 10.1073/pnas.0908317106

SI Experimental Procedures

Protein Expression and Sample Preparation. Syb(1–96) and Syb(1–116) from *Rattus norvegicus* were expressed in BL21(DE3) or BL21(DE3)RIL cells under the control of the T7 promoter (pET28a), and purified essentially as described in refs. 1 and 2. Isotope labeling was accomplished in M9 media with $(^{15}NH_4)_2SO_4$ and ^{13}C-labeled glucose as the sole ^{15}N and ^{13}C sources. Syb(1–96) was purified without the presence of detergent, whereas Syb(1–116) was purified in the presence of 1% sodium cholate. The shorter membrane-bound fragment Syb(60–116) was produced from Syb(1–116) by proteolytic cleavage with botulinum neurotoxin D as described in ref. 3. Fig. S7 demonstrates protein purity.

For proteins with TM domains [i.e., Syb(1–116) and Syb(60–116)], detergent exchange was carried out on the Ni affinity column to replace sodium cholate with dodecylphosphocholine (DPC). The final NMR samples contained 1 mM protein and 200 mM DPC in 20 mM Mes, pH 6.0 buffer with 150 mM NaCl, 5 mM DTT, and 1 mM EDTA. These samples were stable for extended periods of time at measuring temperatures of 45 °C. Since soluble Syb(1–96) was prone to aggregation at high concentration and elevated temperatures, protein concentrations were limited to 0.2 mM in 60 mM phosphate, pH 6.1 buffer with 300 mM NaCl, 5 mM DTT, and 1 mM EDTA and subsequent NMR experiments were performed at 18 °C. Long exposures to higher temperatures lead to irreversible protein aggregation. The Syb(1–96)/DPC sample was made by direct addition of an appropriate amount of DPC powder to the aqueous Syb(1–96) sample. The final sample containing 0.5 mM protein and 300 mM DPC was stable in the 60 mM phosphate, pH 6.1 buffer with 300 mM NaCl, 5 mM DTT, and 1 mM EDTA when measured at 45 °C.

Sample Optimization for NMR Spectroscopy. Based on earlier NMR studies of Syb(1–96) in solution and anticipated experimental challenges with the small dispersion of a partially unfolded integral membrane protein in large DPC micelles, we first studied the shorter membrane-bound fragment Syb(60–116). HSQC and selected backbone triple-resonance spectra were recorded with samples at different protein:lipid ratios and temperatures ranging from 25 to 50 °C. Ultimately, we found that a protein:lipid ratio of 1:200 and a recording temperature of 45 °C gave the best resolved spectra while keeping the sample stable for extended measurement times. TROSY was not beneficial for this partially flexible protein. Several resonances gradually disappeared when the temperature was lowered, presumably due to slow conformational exchange. A fully assigned ^{15}N-^{1}H HSQC spectrum of Syb(60–116) in DPC micelles and recorded at 45 °C is shown in Fig. S1.

NMR Spectroscopy. Three-dimensional backbone experiments [HNCA (4), HNCACB (5), HNCO (4), HN(CA)CO (6), CBCA(CO)NH (7), and HNHA (8)] of Syb(1–116) were collected on a Varian Unity Inova 600 MHz NMR spectrometer. Additional 3-D experiments to aid with side-chain assignments [HCCH-TOCSY (9), (H)CC(CO)NH, H(CC)(CO)NH, (10) and HBHA(CO)NH (11)] were collected on a Bruker Avance 800 MHz spectrometer. Some HSQC and triple-resonance spectra of Syb(60–116) were collected on a Bruker Avance 600 MHz spectrometer. All three spectrometers were equipped with cryoprobes. ^{15}N-edited NOESY spectra with a mixing time of 120 ms and heteronuclear $\{^{1}H\}$-^{15}N NOE, ^{15}N-T_1, and T_2 measurements (12) were collected at 800 MHz. A 5 s saturation delay was used in the heteronuclear NOE experiment. Relaxation delay times of 10, 60, 120, 220, 400, 500, 1000, and 2000 ms and 20, 40, 80, 100, 150, 200, 300, and 400 ms were used in the T_1 and T_2 experiments, respectively. Water-amide proton exchange experiments were performed using the CLEANEX-PM pulse sequence (13) with exchange delays of 5, 10, 20, 40, 80, and 160 ms. All spectra were processed and analyzed with NMRPipe (14) and Sparky (15). Indirect dimensions in the 3-D experiments were processed with forward-backward linear prediction.

Secondary Chemical Shifts and Hydropathy Analysis. Secondary chemical shifts were evaluated as described in ref. 16: $(\Delta C\alpha - \Delta C\beta)_i$ was calculated as $1/3(\Delta C^{\alpha}_{i-1} + \Delta C^{\alpha}_{i} + \Delta C^{\alpha}_{i+1} - \Delta C^{\beta}_{i-1} - \Delta C^{\beta}_{i} - \Delta C^{\beta}_{i+1})$. The Membrane Protein Explorer (http://blanco.biomol.uci.edu/mpex) was used to assess the hydropathy and amphipathic nature of synaptobrevin. The octanol scale and a 15-residue sliding window were used for hydrophobic moment calculation.

Structure Calculations of Syb(1–116). Dihedral angle restraints were predicted from the TALOS program (17) based on the experimental Cα, Cβ, CO, N, and Hα chemical shift inputs. NOE distances extracted and calibrated from ^{15}N-edited NOESY spectra with the PASD (18) routine in Xplor-NIH (19) were used for structure calculation. All NOE assignments were manually checked. An HNHA experiment was performed to measure $^{3}J_{HN}$ and $^{3}J_{H\alpha}$ couplings in hopes of obtaining additional dihedral angle restraints. However, although reduced in the helical regions, the J-coupling constants could not be precisely measured due to spectral overlap, which precluded their use in structure calculations. Alpha-helical backbone hydrogen bond distance restraints were used for residues 42–49 and 94–115 because chemical shifts, NOE's, and a lack of amide hydrogen-exchange indicated stable α-helices in these regions. One hundred structures were calculated in Xplor-NIH. The final 20 structures were selected based on the lowest NOE and dihedral angle violations and covalent energies. The Ramachandran plot statistics yielded: most favored, 78.0%; allowed, 13.5%; generously allowed, 6.1%; disallowed, 2.4%.

1. Fasshauer D, Eliason WK, Brunger AT, Jahn R (1998) Identification of a minimal core of the synaptic SNARE complex sufficient for reversible assembly and disassembly. *Biochemistry* 37:10354–10362.
2. Schuette CG, et al. (2004) Determinants of liposome fusion mediated by synaptic SNARE proteins. *Proc Natl Acad Sci USA* 101:2858–2863.
3. Yamasaki S, et al. (1994) Cleavage of members of the synaptobrevin/VAMP family by types D and F botulinal neurotoxins and tetanus toxin. *J Biol Chem* 269:12764–12772.
4. Grzesiek S, Bax A (1992) Improved 3D triple-resonance NMR techniques applied to a 31-kDa protein. *J Magn Reson* 96:432–440.
5. Wittekind M, Mueller L (1993) HNCACB, a high-sensitivity 3D NMR experiment to correlate amide-proton and nitrogen resonances with the alpha-carbon and beta-carbon resonances in proteins. *J Magn Reson B* 101:201–205.
6. Clubb RT, Thanabal V, Wagner G (1992) A constant-time 3-dimensional triple-resonance pulse scheme to correlate intraresidue H-1(N), N-15, and C-13(') chemical-shifts in N-15-C-13-labeled proteins. *J Magn Reson* 97:213–217.
7. Grzesiek S, Bax A (1992) Correlating backbone amide and side-chain resonances in larger proteins by multiple relayed triple resonance NMR. *J Am Chem Soc* 114:6291–6293.

8. Vuister GW, Bax A (1993) Quantitative J correlation - a new approach for measuring homonuclear 3-bond J($H^N H^\alpha$) coupling-constants in ^{15}N-enriched proteins. *J Am Chem Soc* 115:7772–7777.
9. Kay LE, et al. (1993) A gradient-enhanced HCCH TOCSY experiment for recording side-chain H-1 and C-13 correlations in H2O samples of proteins. *J Magn Reson B* 101:333–337.
10. Montelione GT, Lyons BA, Emerson SD, Tashiro M (1992) An efficient triple resonance experiment using C-13 isotropic mixing for determining sequence-specific resonance assignments of isotopically-enriched proteins. *J Am Chem Soc* 114:10974–10975.
11. Grzesiek S, Bax A (1993) Amino acid type determination in the sequential assignment procedure of uniformly 13C/15N-enriched proteins. *J Biomol NMR* 3:185–204.
12. Kay LE, Torchia DA, Bax A (1989) Backbone dynamics of proteins as studied by 15N inverse detected heteronuclear NMR spectroscopy: Application to staphylococcal nuclease. *Biochemistry* 28:8972–8979.
13. Hwang TL, van Zijl PC, Mori S (1998) Accurate quantitation of water-amide proton exchange rates using the phase-modulated CLEAN chemical EXchange (CLEANEX-PM) approach with a Fast-HSQC (FHSQC) detection scheme. *J Biomol NMR* 11:221–226.
14. Delaglio F, et al. (1995) NMRPipe: A multidimensional spectral processing system based on UNIX pipes. *J Biomol NMR* 6:277–293.
15. Goddard TD, Kneller DG (2008) SPARKY 3, NMR Assignment and integration Software (University of California, San Francisco), Version 3.114.
16. Metzler WJ, et al. (1993) Characterization of the three-dimensional solution structure of human profilin: 1H, 13C, and 15N NMR assignments and global folding pattern. *Biochemistry* 32:13818–13829.
17. Cornilescu G, Delaglio F, Bax A (1999) Protein backbone angle restraints from searching a database for chemical shift and sequence homology. *J Biomol NMR* 13:289–302.
18. Kuszewski JJ, Thottungal RA, Clore GM, Schwieters CD (2008) Automated error-tolerant macromolecular structure determination from multidimensional nuclear Overhauser enhancement spectra and chemical shift assignments: Improved robustness and performance of the PASD algorithm. *J Biomol NMR* 41:221–239.
19. Schwieters CD, Kuszewski JJ, Tjandra N, Clore GM (2003) The Xplor-NIH NMR molecular structure determination package. *J Magn Reson* 160:65–73.

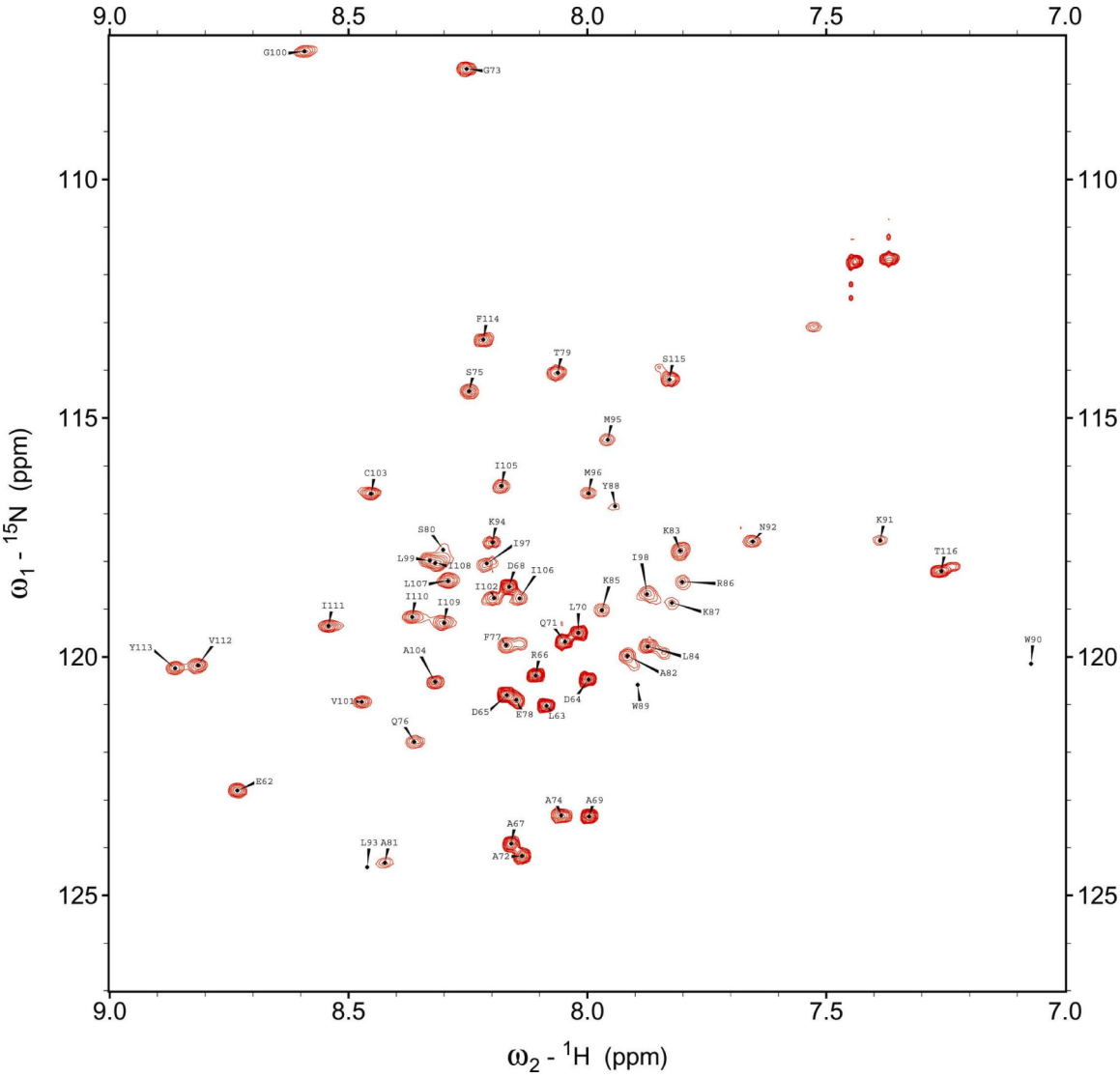

Fig. S1. ^{15}N-^{1}H HSQC spectrum of Syb(60–116) in DPC micelles at pH 6.0 and 45 °C, measured at 600 MHz. Assignments of backbone amides are denoted by one letter amino acid abbreviations followed by their sequence numbers. Assignments have been deposited in Biological Magnetic Resonance Data Bank (BMRB ID code: 16512).

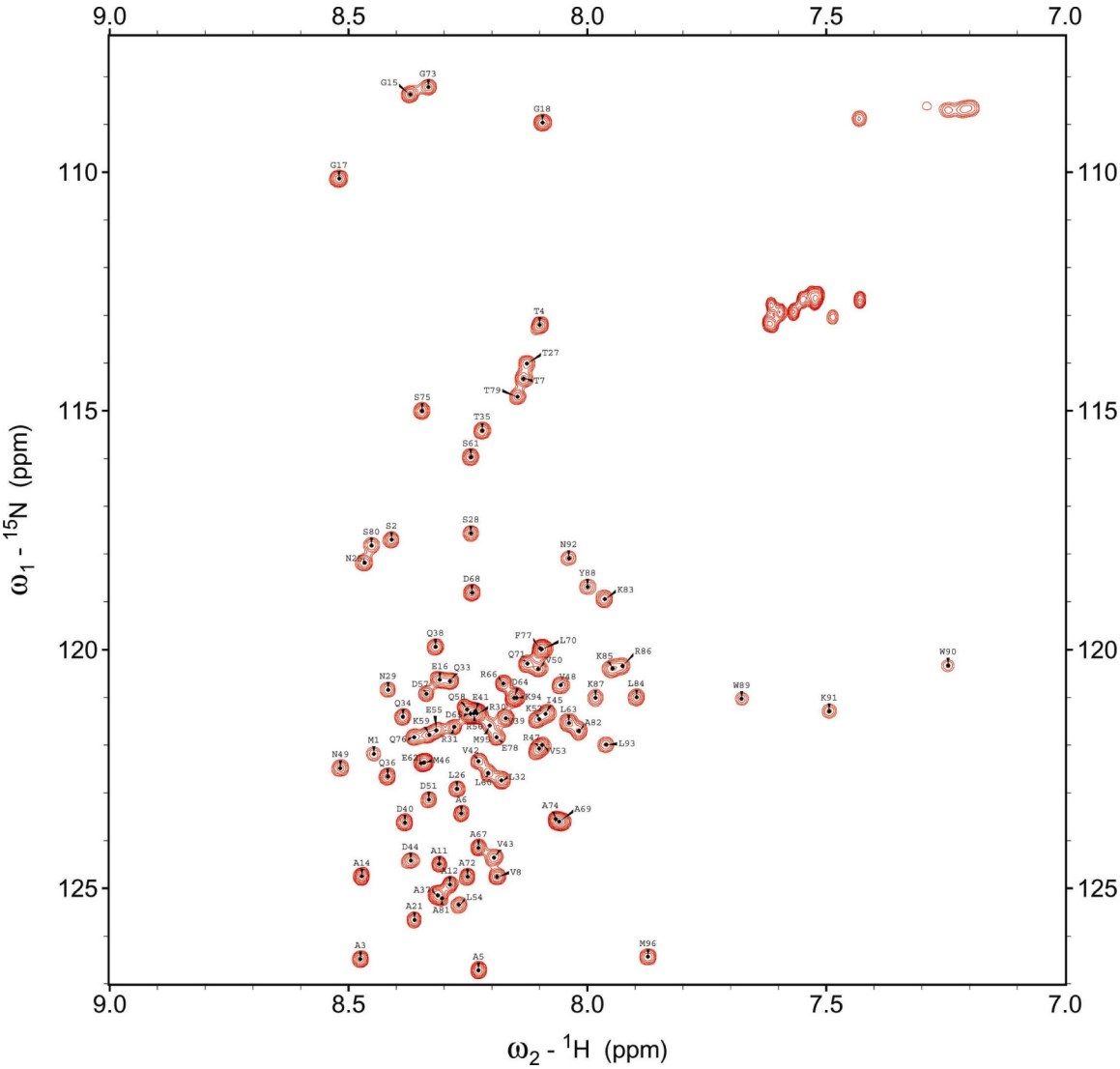

Fig. S2. ^{15}N-^{1}H HSQC spectrum of Syb(1–96) in buffer at pH 6.1 and 18 °C, measured at 600 MHz. Assignments of backbone amides are denoted by one letter amino acid abbreviations followed by their sequence numbers. Assignments have been deposited in Biological Magnetic Resonance Data Bank (BMRB ID code: 16514).

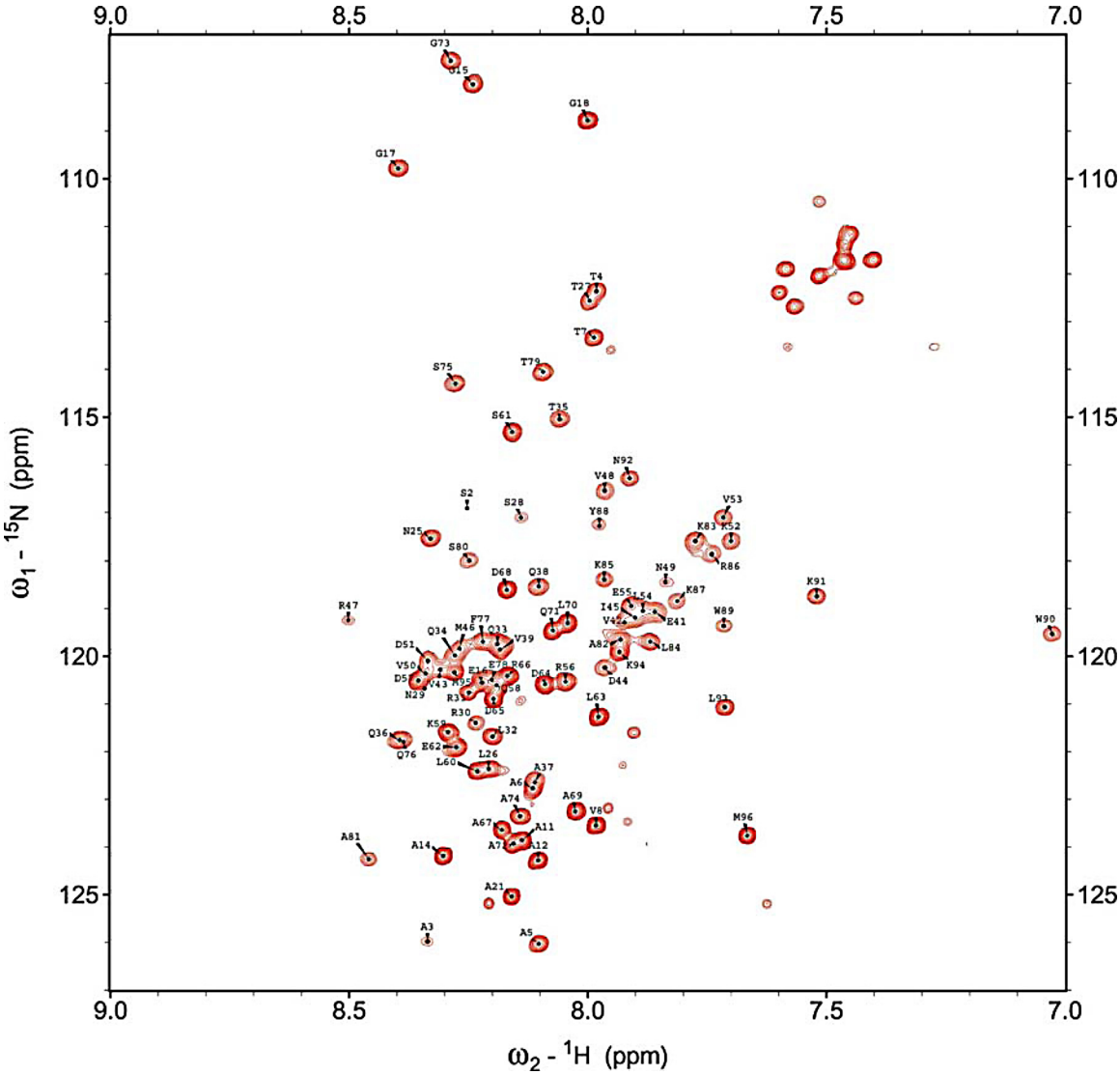

Fig. S3. ^{15}N-^{1}H HSQC spectrum of Syb(1–96) in DPC micelles at pH 6.1 and 45 °C, measured at 800 MHz. Assignments of backbone amides are denoted by one letter amino acid abbreviations followed by their sequence numbers. Assignments have been deposited in Biological Magnetic Resonance Data Bank (BMRB ID code: 16514).

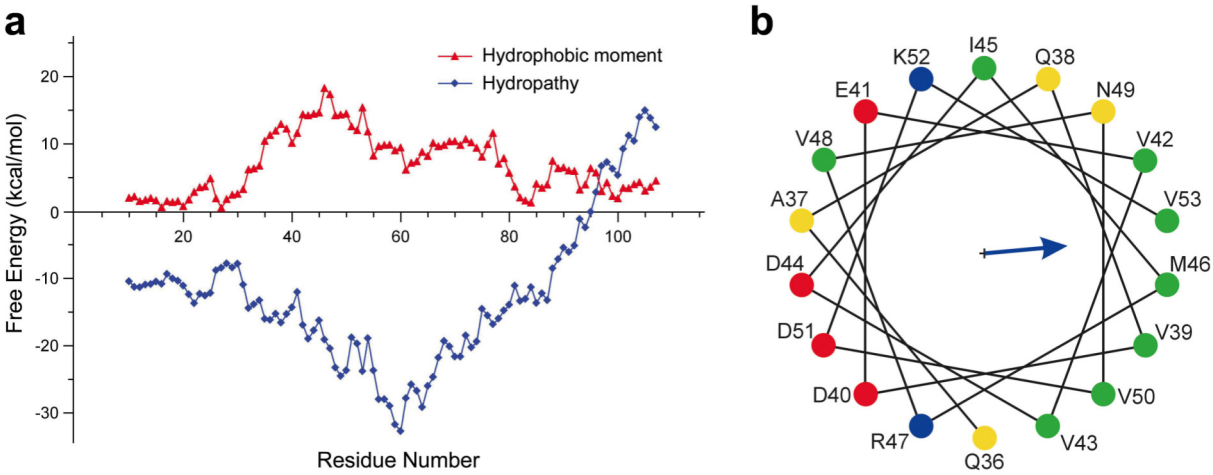

Fig. S4. Hydropathy and helical wheel analysis. (*a*) Hydropathy and hydrophobic moment analysis of Syb1–116. The octanol scale is used for calculation of the free energy of transfer from bilayer to water. A 15-residue window is used for hydrophobic moment calculation. The x-coordinate is the central residue of the window. (*b*) Helical wheel and hydrophobic moment (blue vector = 14.7 kcal/mol) for residues 36–53. Hydrophobic residues: green; neutral hydrophilic residues: yellow; positively charged residues: blue; and negatively charged residues: red.

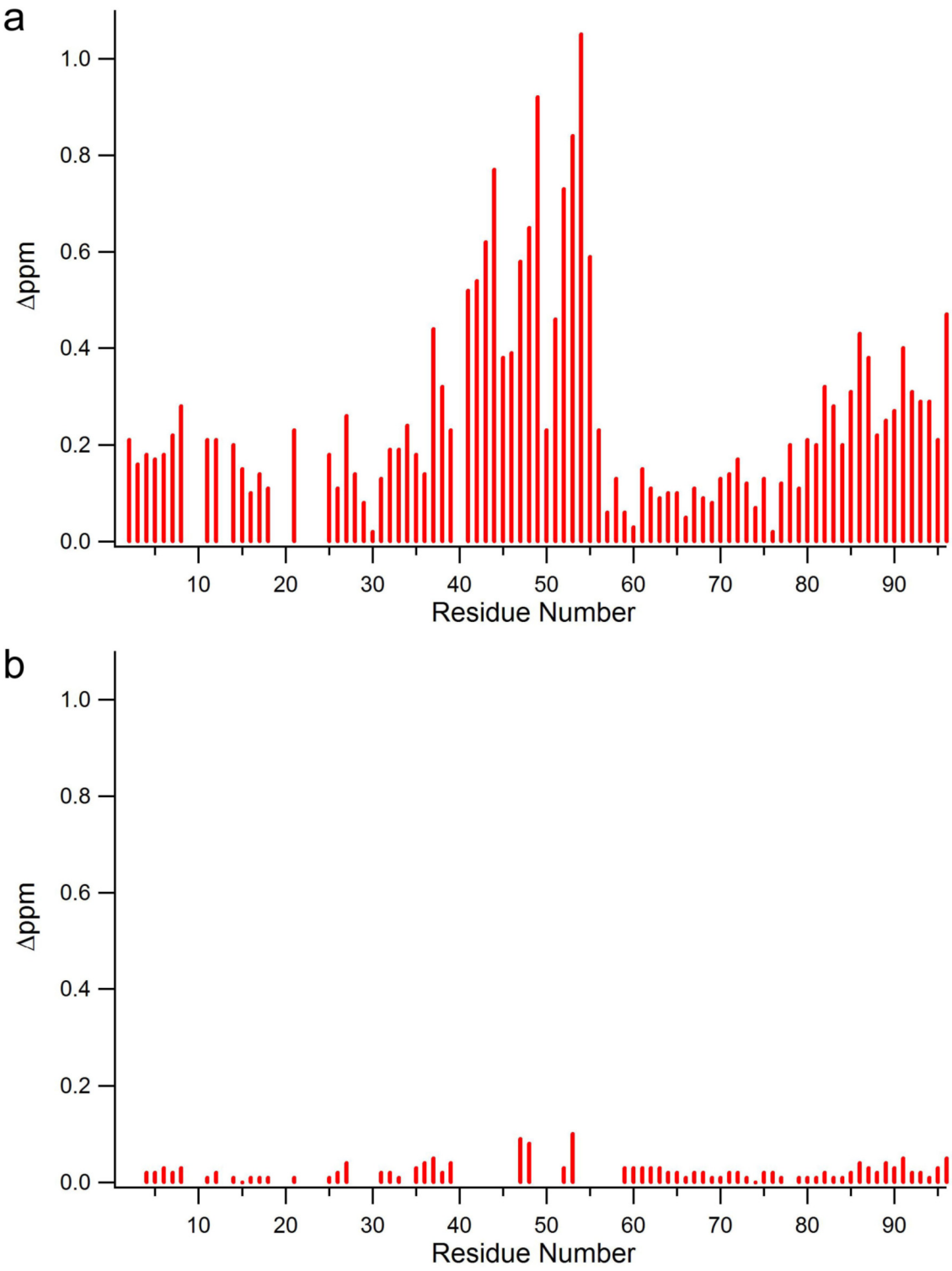

Fig. S5. Combined chemical shift changes of Syb(1–96) in different environments. (*a*) 300 mM DPC versus aqueous buffer; (*b*) 300 mM DPC vs. 30 mM DPC and 4 mM SDS. The chemical shift changes were also measured for 300 mM DPC vs. 300 mM DPC with 40 mM SDS. They were virtually indistinguishable (i.e., the differences were negligible and even smaller than those shown in *b*). Additional chemical shift changes were measured for 300 mM DPC vs. 7.5 mM DPC and 1 mM SDS. The results were indistiguishable from those shown in *b*. The combined chemical shifts, Δppm, are calculated as: $[(\Delta\delta_H)^2 + (w_N\,\Delta\delta_N)^2]^{0.5}$. $\Delta\delta_H$ and $\Delta\delta_N$ are chemical shift changes in ppm, and w_N, the weight factor for nitrogen, is 0.154. [Evenas J, et al. (2001), *J Mol Biol* 309: 961–974.]

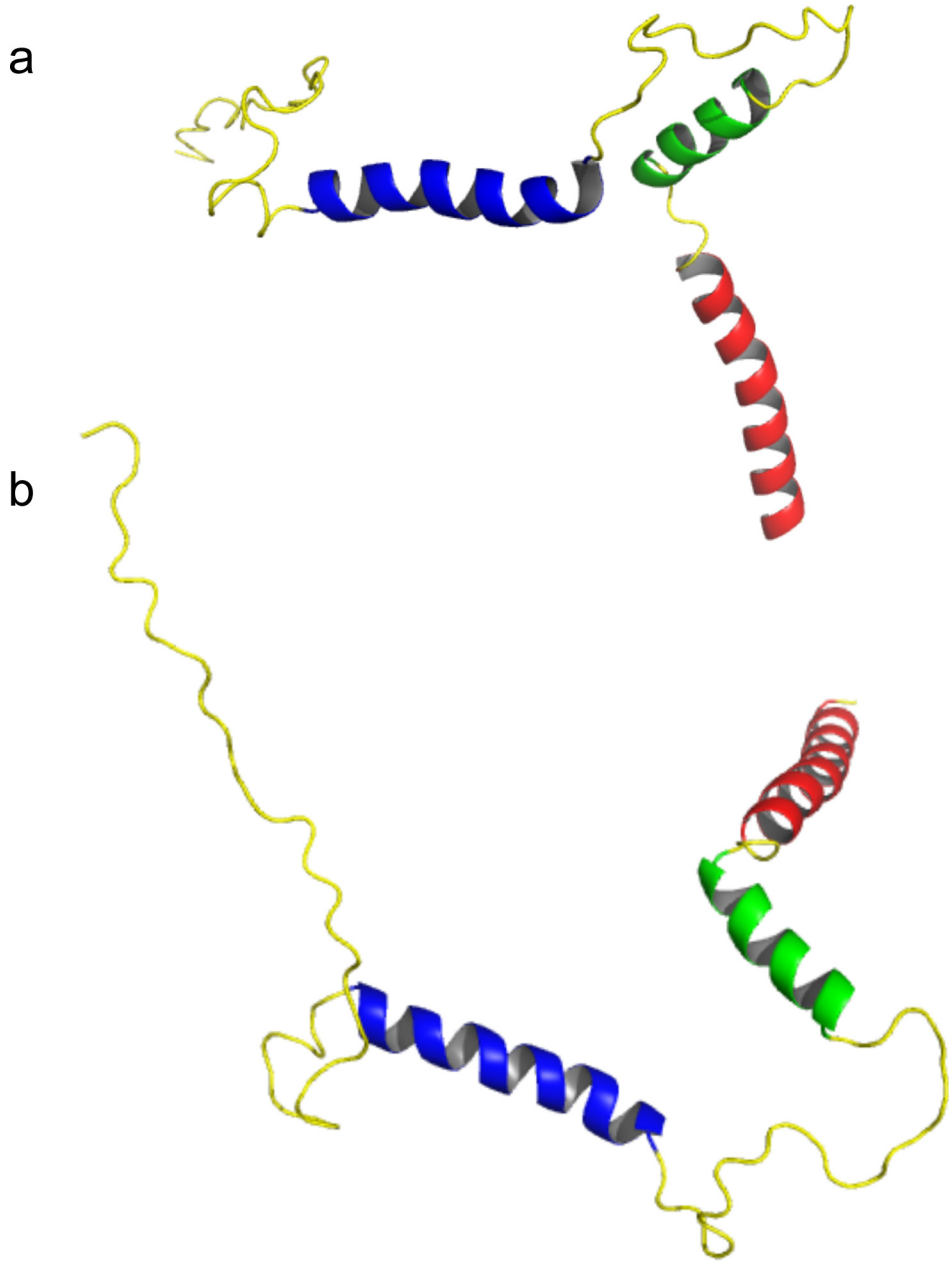

Fig. S6. Lowest energy structure of Syb(1-116) in DPC micelles, (*a*) same as in Fig. 5 in main text, but with residues 1–34 included. (*b*) same as (*a*) but viewed from top approximately perpendicular to micelle (or hypothetical membrane) surface.

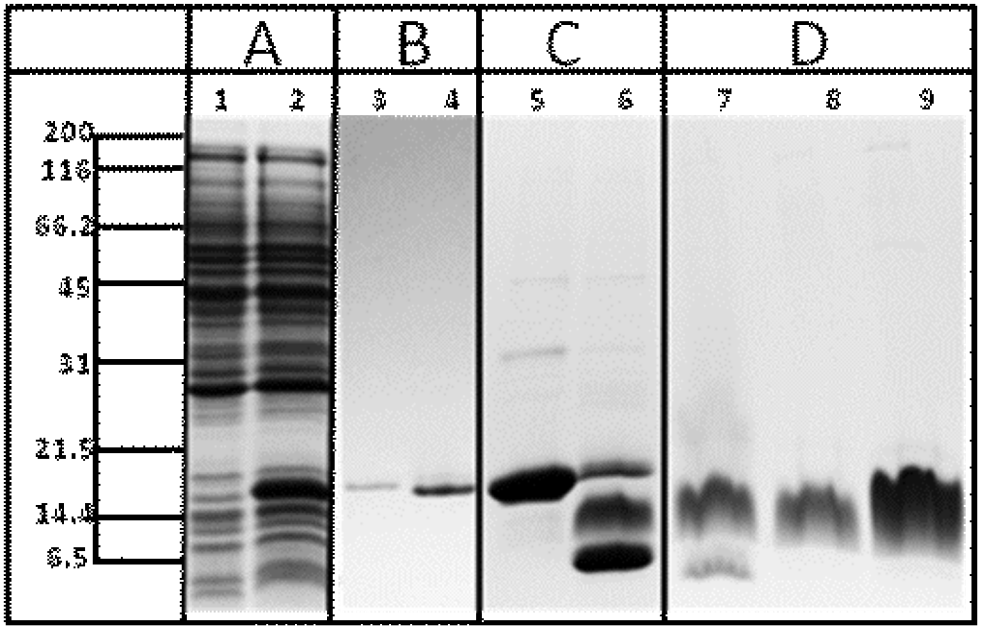

Fig. S7. Summary of synaptobrevin purification. (*A*) Total *E. coli* protein before (1) and after (2) IPTG induction. Overexpressed Syb (actual M_r 13 kDa) runs at apparent M_r of ≈18 kDa. (*B*) Purified synaptobrevin (3) migrates slightly faster after removal of His_6-tag (4); (*C*) Purified synaptobrevin before (5) and during cleavage with BoNT-D (6). The bottom band represents Syb(1–59), the middle band Syb(60–116), and the upper band undigested Syb; (*D*) Completely BoNT-D digested synaptobrevin (7), and immobilized metal affinity chromatography or ion exchange chromatography purified Syb(60–116) (8 and 9). Overloaded lanes (5 and 9) confirm high purity of preparations.

Table S1. NMR and refinement statistics for the synaptobrevin(1–116) structures

	Syb(1–116)
NMR distance and dihedral angle constraints	
Distance constraints	
Total NOE	318
Intra-residue	110
Inter-residue	208
Sequential ($i–j = 1$)	126
Medium-range ($i–j \leq 4$)	79
Long-range ($i–j \geq 5$)	3
Hydrogen bonds	44
Total dihedral angle constraints	
ϕ	55
ψ	55
Structure statistics*	
Violations (mean and SD)	
Distance constraints (Å)	0.051 ± 0.003
Dihedral angle constraints (°)	0.13 ± 0.11
Max. dihedral angle violation (°)	2.95
Max. distance constraint violation (Å)	0.74
Deviations from idealized geometry	
Bond lengths (Å)	0.0027 ± 0.0005
Bond angles (°)	0.413 ± 0.007
Impropers (°)	0.29 ± 0.02
Average pairwise r.m.s. deviation (Å)	
Helix I (36–54): Heavy	1.94 ± 0.36
Backbone	1.03 ± 0.29
Helix II (77–88): Heavy	1.18 ± 0.43
Backbone	0.81 ± 0.29
Helix III (93–115): Heavy	1.41 ± 0.28
Backbone	0.62 ± 0.18

*Calculated from 20 selected lowest energy structures.